First principles calculation of the reaction rates for ligand binding to myoglobin: the cases of NO and CO

Anikó Lábas,[a] Dóra K. Menyhárd,[b] Jeremy N. Harvey,*[c] Julianna Oláh,*[a]

Abstract

Ligand binding by proteins is among the most fundamental processes in nature. Among these processes the binding of small gas molecules, such as O_2, CO and NO to heme proteins has traditionally received vivid interest, which was further boosted by their recently recognized significant role in gas sensing in the body. At the heart of the binding of these ligands to the heme group is the spin-forbidden reaction between high-spin iron(II) and the ligand yielding a low spin adduct. We use computational means to address the complete mechanism of CO and NO binding by myoglobin. As it involves several steps occurring on different time-scales, molecular dynamics simulations were performed to address the diffusion of the ligand through the enzyme, and DFT calculations in combination with statistical rate calculation to investigate the spin-forbidden reaction. The calculations yielded rate constants in qualitative agreement with experiment and revealed that the bottle-neck of NO and CO binding is different: for NO diffusion was found to be rate-limiting, while for CO the spin-forbidden step is the slowest.

Introduction

Ligand binding is essential for life. The process usually involves the migration of the ligand from the surrounding solvent to within the binding site of the protein, followed by the stabilization of the ligand in the binding site. Among these processes the binding of small diatomic gas molecules by heme proteins deserves a special place. Heme proteins evolved to assist aerobic organisms to carry, store and activate O_2.[1] Histidine-ligated

[a]   Anikó Lábas, Dr. Julianna Oláh
        Department of Inorganic Chemistry
        Budapest University of Technology and Economics
        H-1111 Budapest Szent Gellért tér 4., Hungary
[b]   Dr. Dóra K. Menyhárd
        MTA-ELTE Protein Modelling Research Group
        H-1117 Budapest Pázmány Péter st. 1/A, Hungary
[c]   Prof. Jeremy N. Harvey
        Department of Chemistry
        KU Leuven
        B-3001 Leuven Celestijnenlaan 200F- box 2404, Belgium

hemoglobin and myoglobin are responsible for O_2-transport and storage, respectively, while thiolate-ligated cytochrome P450 enzymes activate molecular oxygen by cleaving the O-O bond allowing the organism to perform powerful oxidation reactions in a "safe" environment. The fast reaction occurring between triplet O_2 and Fe(II)-hemes present in their high-spin ground state leading to low-spin oxyhemes has been puzzling scientists for long due to the spin-forbidden nature of the reaction, which requires the flip of at least one electron on the iron centre and a change in the overall spin. Based on DFT calculations it was argued that upon ligand binding the corresponding high-spin and low-spin surfaces approach each other creating a broad crossing region maximizing the cross-over probability.[2]

Apart from O_2, the heme cofactor can bind other small molecules such as nitric oxide (NO) and carbon monoxide (CO), which traditionally were regarded as toxic. However, by now a wealth of evidence has been presented for their physiological regulatory role.[3],[4] When acting as signaling molecules, NO or CO exert their effect via heme-based gas-sensors in the body: association of the gas molecule with (or its dissociation from) the heme group triggers conformational changes leading to signal transduction and the switching on and off of biological functions. Furthermore, heme-based proteins play central roles in gas-generation/reception mechanisms and provide a meeting point for gases to interact.[5]

In order to get a detailed understanding of the factors that influence the binding of gas molecules to heme proteins intensive experimental and theoretical work has been done. On the experimental side, among others, the kinetics of CO and NO addition to various heme proteins[6–13] have been extensively studied and a distinct difference between the rate constants for NO and CO binding and release has been unambiguously found. The rate constant for NO binding is close to the diffusion limit[4] (see selected examples in Table 1), superseding that for CO binding by several orders of magnitude.

Table 1. Binding (k_{on}) and dissociation (k_{off}) rate constants and the equilibrium constant for the reaction of diatomic gas molecules with selected ferrous heme proteins

Protein	Ligand	k_{on} [M^{-1} s^{-1}]	k_{off} [s^{-1}]	K_{eq} [M^{-1}]	Ref.

myoglobin	NO	$1.7 \cdot 10^7$	$1.2 \cdot 10^{-4}$	$1.4 \cdot 10^{11}$	[8]
myoglobin	NO	$2.2 \cdot 10^7$	*ND*	*ND*	[9]
myoglobin	O_2	$1.7 \cdot 10^7$	15	$1.1 \cdot 10^6$	[9]
myoglobin	CO	$5.1 \cdot 10^5$	$1.9 \cdot 10^{-2}$	$2.7 \cdot 10^7$	[9],[14]
hemoglobin	NO	$2.5 \cdot 10^7$	$4.6 \cdot 10^{-5}$	$5.3 \cdot 10^{11}$	[8]
sGC[b]	CO	$4 \cdot 10^4$	10.7	$1.2 \cdot 10^{-4}$	[10]
sGC[b,c]	NO	$1.4 \cdot 10^8$	$6 \cdot 10^{-4}$	$2.3 \cdot 10^{11}$	[11–13]

ND: not determined,

[b] Soluble Guanylyl Cyclase [calc as kon/koff from refs. [11–13]

Computational chemists addressed the problem of NO and CO binding to heme proteins from two distinct angles due to the complex nature of the ligand binding process.

Ligand diffusion and the internal motions of the protein have been studied using molecular dynamics simulations in which the whole protein structure, the ligand molecules and the surrounding solvent can be explicitly described. However, due to the extended timescales needed for the modelling of the diffusion process it was the advent of GPU-accelerated MD simulations techniques which boosted research in this field yielding reasonable rate constants for ligand diffusion to myoglobin,[15–21] and to nitrogenase/ hydrogenase enzymes.[22–24] However, as classical molecular dynamics simulations do not treat electrons explicitly they are inherently unable to describe chemical reactions. Therefore, the ligand binding process has been addressed by quantum chemists concentrating on a small model of heme enzymes: typically on a porphine-based model of the heme complex. These studies significantly contributed to

our understanding of the spin-state energetics of various porphine-based model systems,[25–30] the binding energies of small ligand molecules to heme[31] and a few studies explicitly addressed the spin-forbidden reaction as well.[32–34]

The aim of the present work is to calculate absolute rate-constants for protein-ligand reactions from first principles calculations. According to the best of our knowledge this is the first study to report such calculations. For our study we chose NO and CO binding[14] to myoglobin as (1) myoglobin is the most studied model within the group of heme proteins; (2) these processes are well-characterized experimentally, thus reliable reference data are available; (3) binding involves spin-forbidden chemical reactions; and (4) the measured rate constants for NO and CO binding are distinctly different.

In our work we divide the overall reaction into two main steps and determine the rate constant for each step separately (see Figure 1). (1) Diffusion of the ligand in and out (k_1 and k_{-1}) of the heme pocket is studied with molecular dynamics simulations and (2) the spin-forbidden chemical reaction (k_2 and k_{-2}) is investigated with density functional theory and non-adiabatic transition state theory calculations using a model of the heme pocket. These two steps together account for the overall process of ligand binding by myoglobin. Finally, we combine the obtained results to predict the overall rate constant for the reactions (k_{on} and k_{off}).
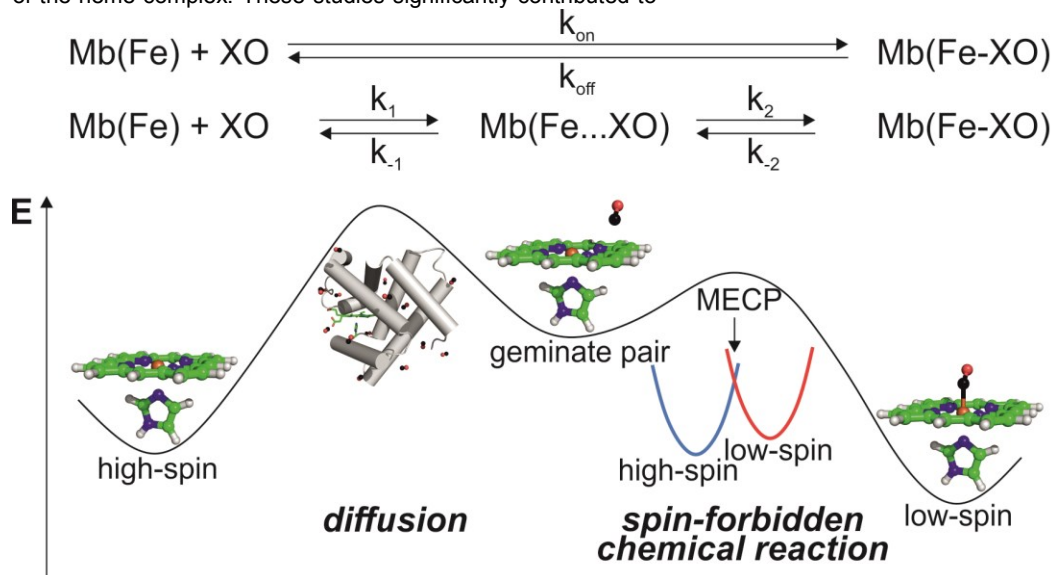

Figure 1. Schematic representation of XO (NO or CO) binding by myoglobin. The resting state of myoglobin is high-spin deoxymyoglobin. Diatomic gas molecules diffuse in to the heme pocket forming the geminate pair which can undergo recombination with the heme group yielding low-spin nitroxy or carbonmonoxy myoglobin. The recombination process is spin-forbidden and the reaction proceeds through the minimum energy crossing point (MECP) between the high-spin and low-spin potential energy surfaces.

Results and Discussion

Ligand diffusion in myoglobin.

The diffusion of ligands into myoglobin has been extensively studied by mutagenesis[35–37], X-Ray diffraction experiments[16,38] and molecular dynamics simulations[21,39],[40], just to mention some of the studies. These confirmed the presence of 4 xenon or gas storing cavities in myoglobin first identified by Tilton,[41] and shed light on the pathways of ligand migration to the heme pocket. By now it is well-established that the majority of the ligands enter and exit the protein through the so-called His-gate, a channel positioned directly above the heme propionate side chains, that opens upon outward movement of the His64 side chain.[37] However MD simulations[36,42] and random mutagenesis studies[43] point to the existence of other ligand migration routes as well.
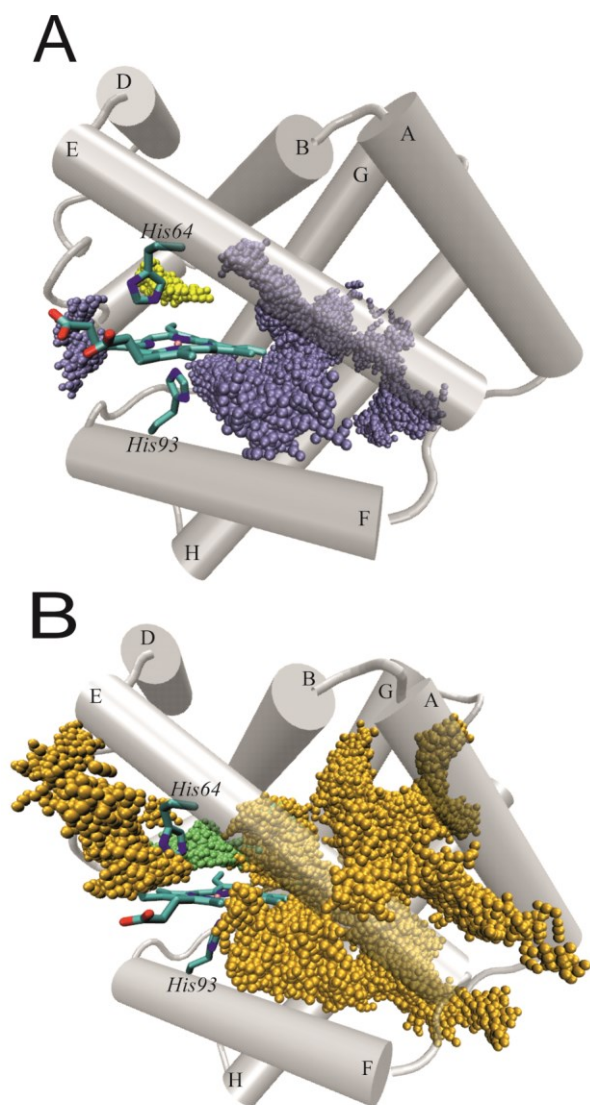

Figure 2. Migration routes for CO (A) and for NO (B) observed in the MD simulations. Ligand positions observed in the heme pocket are depicted in yellow for CO and in green for NO. The His-gate (His64), the heme group and the axial histidine residue are shown in licorice.

Here, we are primarily interested in predicting the rate constant for the diffusion process. We performed 300 ns long MD simulations on solvated myoglobin systems in the presence of 40 CO or NO molecules. In the case of NO the simulations were performed using various water models (TIP3P, TIP4P, TIP4P/2005[44], TIP4Pew[45] and OPC[46]), while in the case of CO binding the TIP4P and OPC models were used. The simulation with the OPC model was 635 ns long. Next, we clustered the structures visited in the trajectories and visually inspected the routes followed by the ligands. As expected ligands primarily reached the heme pocket via the His-gate, however we found evidence for ligands entering the protein between the meeting points of helices E-F and G-H as well (see Fig. 2). In the first case ligands could reach the active site directly from the solvent, while in the latter case their migration routes included the Xe-binding pockets as well. The Xe-binding cavities were occupied by ligands in the majority of the simulation time, however, their occupancy depended upon the used water model (see Table S1 in the supporting information).

The third step of our analysis was to build our coarse-grained kinetic model (see the SI for detailed information). To each NO/CO molecule at each structure of the trajectory we assigned one of the following states: (1) solvent phase (2) anywhere in the protein with the exception of the heme pocket (3) heme pocket. After this we counted the number of events in which an NO/CO molecule reached the heme pocket from the solvent and returned to the bulk phase again. Using the analysis described in the SI, we converted these event counts into rate constants for diffusion (k_1 and k_{-1}, Table 2). The rate for entry (k_1) in the case of NO diffusion is predicted to be between $1.7 \cdot 10^8$ and $4.7 \cdot 10^8$ $M^{-1}s^{-1}$, depending on the solvent model used. These values are all roughly one order of magnitude larger than the experimental entry rate[14] for NO and O_2 in myoglobin (35 $\mu M^{-1}s^{-1,[14]}$). In the case of CO we obtained a rate constants of $6 \cdot 10^7$ -$1.1 \cdot 10^8$ $M^{-1}s^{-1}$ which are only about 4.5-9 times larger than the experimental rate constant (12 $\mu M^{-1}s^{-1,[37]}$) and smaller than the values (k_1:646 $\mu M^{-1}s^{-1,[15]}$ and 306,7 $1/\mu Ms^{-1,[47]}$) obtained from more elaborate Markov-state models, which describe all potential ligand migration routes in the protein. Our rate constants reproduce the experimental trend that CO migrates into the heme pocket more slowly than does NO: This may partly originate from the fact that the van der Waals radii of the atoms of CO are slightly larger than those of NO. Our results also yield near-quantitative agreement with experiment regarding the equilibrium constant for 'binding' of NO within the heme pocket, with calculated values ranging between 2.2 and 3.4 vs the experimental value of 3.2. In the case of CO the agreement is slightly worse, which most likely originates from the poor sampling of the slower CO diffusion processes in our simulations. The good correspondence among the values obtained with various solvent models suggests that the viscosity of the water models plays a minor role in determining the calculated rate constant for the diffusion of gas molecules in contrast to what was suggested earlier.[15]

Table 2. Calculated rate constants and equilibrium constant and number of in-out events for NO and CO diffusion in myoglobin from 300ns long MD simulations.

Experimental data and previous computed results are given for reference values.

ligand	water model	k_1 (M^{-1} s^{-1})	k_{-1} (s^{-1})	$K(k_1/k_{-1}, M^{-1})$	$N^{\underline{o}}_{in-out}$
CO	TIP4P	$6 \cdot 10^7$	$2 \cdot 10^8$	0.3	5
	OPC£	$1.1 \cdot 10^8$	$2.5 \cdot 10^8$	0.44	21
NO	TIP3P	$3.6 \cdot 10^8$	$1.3 \cdot 10^8$	2.7	32
	TIP4P	$4.7 \cdot 10^8$	$1.8 \cdot 10^8$	2.6	39
	TIP4P/2005	$2.2 \cdot 10^8$	$6.3 \cdot 10^7$	3.4	18
	TIP4Pew	$3.4 \cdot 10^8$	$1.2 \cdot 10^8$	2.9	27
	OPC	$1.8 \cdot 10^8$	$8.0 \cdot 10^7$	2.2	15

experimental values or previous computed values

		k_1	k_{-1}	$K(k_1/k_{-1})$	ref.
O_2		$3.8 \pm 0.9 \cdot 10^7$	$1.2 \pm 0.2 \cdot 10^7$	3.2	[14]
NO/O_2		$3.5 \cdot 10^7$			[9]
CO		$1.2 \cdot 10^7$	$0.53 \cdot 10^7$	2.2	[14]
CO	TIP3P	$3.067 \cdot 10^8$	$1.36 \cdot 10^7$	22	[47]
CO	TIP3P	$6.46 \cdot 10^8$	$1.50 \cdot 10^7$	43	[15,47]

£ this was a 635ns long simulation

Spin-forbidden chemical reaction

The rate constant for binding of the NO or CO ligand to the heme group from within the pocket can be modeled based on the shapes of the relevant potential energy surfaces for the different spin states. There have been many previous calculations both in the case of CO and NO, in fact too many for it to be possible to cite all of them here. Previous work in our groups has addressed both the CO[33,34,48] and NO[49] cases. In these studies, the potential energies for interaction between NO and CO and a small iron-porphyrin-imidazole model of the heme group in proteins such as myoglobin were considered. The iron-porphyrin-imidazole species has low-lying quintet, triplet and singlet electronic states, and the relative energy of these states was calculated using density functional theory, with hybrid functionals such as B3LYP and B3PW91 appearing to agree well with experiment. For example, these functionals confirm that the quintet state is the ground state. In some of our work[32,49] two small models of the heme group were additionally used in conjunction with coupled-cluster theory (CCSD(T)) to attempt to further calibrate the accuracy of B3LYP. These calculations suggested that B3LYP and B3PW91 are indeed reasonably accurate for energetics in this system, with the exception of the binding energy of NO, which was found to be underestimated by roughly 8 kcal/mol.

As well as considering the energetics, minimum energy crossing points between surfaces of different spin were located for CO binding[32-34] and used to rationalize the rate of ligand binding. As mentioned, heme itself has a quintet ground state, but the

CO ligand only binds strongly to the excited singlet state. The singlet state was found to cross the quintet state 2.4 kcal/mol above the energy of separated quintet heme and CO at the B3LYP level.[34] A non-adiabatic form of TST (NATST)[50] was used to compute the rate constant for binding through this MECP[33], yielding a value of 2.8×10^5 s^{-1} at room temperature. As noted in that study, this value relies on a number of assumptions, changes in which could lead to changes in the predicted rate constant by one order of magnitude or more. However, the value agrees well with experimental observations whereby recombination occurs on the μs timescale at room temperature.[51,52]

Many other groups have studied some aspects of heme spin-forbidden ligand addition. In one important recent study, the accuracy of different DFT functionals for the relative energies of singlet, triplet and quintet states of the porphyrin-iron-imidazole system was carefully considered based on a very systematic set of benchmark CCSD(T) calculations.[25] In this study, it was concluded that the relative energy of the triplet and singlet states was of 3.0 and 4.6 kcal/mol, respectively, with an implied error bar of at most 3-4 kcal/mol arising from the various approximations.

As no previous study has involved application of NA-TST to NO addition, we decided to carry out calculations estimating the rate constant for NO addition from the protein pocket surrounding the heme group. For reference, the calculations for CO have been repeated using the same updated electronic structure and NATST methodology. As in our previous work, we have used DFT. However, as it has been shown[53] that dispersion effects can change the bond energy for NO and CO by up to 10 kcal/mol, we have used dispersion-corrected DFT throughout. Test calculations were used to determine a flexible yet compact basis set that reproduces results obtained with very large polarized and augmented triple-zeta basis sets. Also, care was taken to locate the structure and electronic structure of lowest energy for each spin state, taking into account also C_S symmetry where appropriate. Table 3 shows the resulting energies.

The inclusion of dispersion corrections does not strongly affect the relative energies of the different spin states for the heme fragment, with the quintet lying lowest, followed by the triplet and singlet, as in previous studies. Compared to the new CCSD(T) benchmark,[25] it does however seem that B3PW91 slightly exaggerates the stability of the triplet, which lies *lower* in energy than the quintet prior to including the zero-point energy correction. The benchmark study, which does not account for zpe, predicts it should lie 3.0 kcal/mol above the quintet. This is again a reminder that computed energies in this type of system have uncertainties of a few kcal/mol.

Table 3. Calculated relative energies (in kcal/mol) with and without ZPE correction of studied heme models. Fe-X distance is given in Å and X indicates C or N of CO or NO

	B3PW91-D3BJ	+ ZPE	r(Fe-X)/Å
^{5}heme + CO or NO	0.0	0.0	/

^{3}heme	-0.5	0.7	/
^{1}heme	4.2	6.3	/
^{5}heme—CO	-6.7	-6.1	2.55
^{3}heme—CO	-7.0	-5.4	2.55
^{1}heme-CO	-27.0	-22.7	1.77
^{6}heme—NO	-5.3	-4.8	2.94
^{4}heme—NO	-7.4	-5.2	2.35
^{2}heme—NO	-21.2	-17.5	1.76
^{1,5}MECP CO	-4.8	-4.8	2.22
^{2,4}MECP NO	-6.9	-5.3	2.48

The ligand binding energies calculated here differ more strongly from some previously reported values,[34] due to the aforementioned effect of the dispersion correction. The bound forms have singlet and doublet ground states for CO and NO, as in previous work – but they are somewhat lower in relative energy compared to the separated fragments. Furthermore, the inclusion of dispersion means that also on the higher-spin states, there are local minima in which the ligand interacts mostly dispersively with the metal and porphyrin. For CO, these triplet and quintet states involve barely modified electron distributions around the metal, and long Fe-C distances (coincidentally identical within 2 decimals for both cases). The quintet adduct is lower in energy than the triplet adduct. The potential energy well for these dispersively-bound species is quite broad: for the quintet adduct, optimization using an Fe-C distance increased from 2.55 to 3.05 Å leads to an increase in energy of just 0.5 kcal mol^{-1}.

For NO, the sextet state, involving four unpaired electrons at iron and one on the NO moiety, is likewise basically unperturbed compared to the quintet fragment. The quartet adduct, which lies *below* the sextet adduct, involves effectively two unpaired electrons at iron, and one at NO. Hence it appears to correlate to the triplet state of the bare heme. However, upon increasing the Fe-N distance, the energy converges without a barrier towards that of the separated NO and quintet heme, as the Kohn-Sham 'wavefunction' smoothly switches over to alternative spin-pairing, with four unpaired electrons at Fe and an antiferromagnetically coupled electron at NO. Hence this quartet can be formed without spin state change upon NO binding to quintet heme.
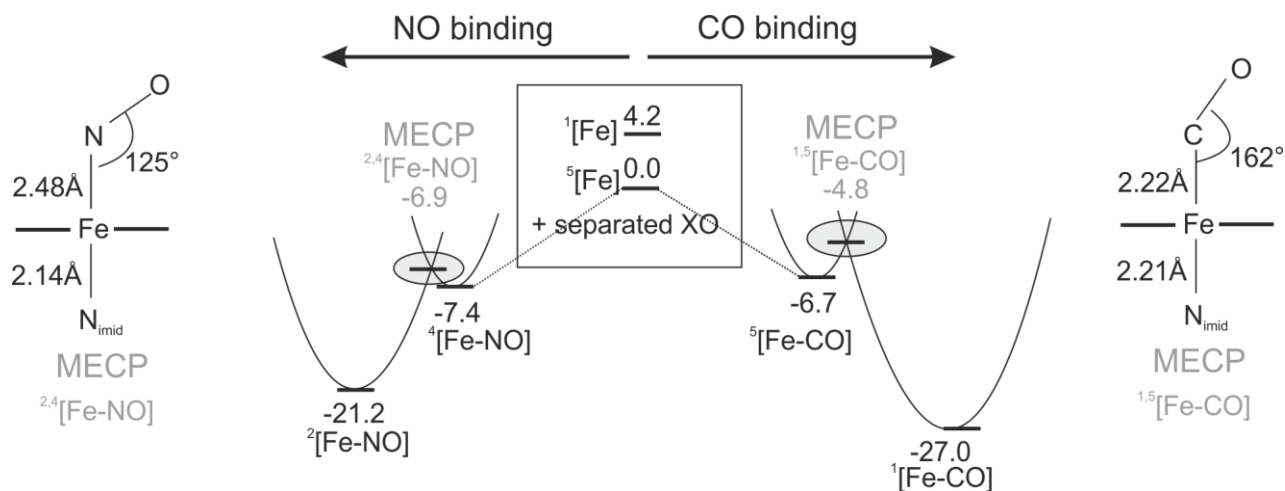

Figure 3. Schematic representation of the potential energy surfaces (minima and MECPs located at the B3PW91-D3BJ level) and most important geometric parameters of MECPs relevant for XO (CO or NO) binding by myoglobin. When the ligand approaches the high-spin heme group, they first form a weakly bound adduct, which rearranges via the MECP to yield the strongly-bound low-spin adduct. Please note, that the scheme is not proportional and parabolas and the dotted lines are only drawn to guide the eye. Numbers represent the relative energies of the species in kcal/mol with respect to the separated heme fragment and XO ligand.

We now turn to the NATST calculation of binding rate constants, for the spin-state change. The reactant state here is the protein with the ligand (NO or CO) in the distal pocket above the heme group. The free energy of this state relative to the state in which the ligand is in the solvent is determined by the rate constants for entry and exit of the ligand determined in the molecular dynamics part. Here we want to know the rate constant for metal-ligand bond formation. This step involves a change in spin state, since the uncoordinated heme has a quintet ground state and the bound form has either a singlet (CO) or doublet (NO) ground state. The bottleneck for this step is therefore an MECP between the relevant potential energy surfaces. As discussed above, the NO ligand can interact in a barrierless way with the heme group to form a weakly bound quartet state, so the relevant MECP is between the quartet and doublet states, ^{2,4}MECP NO in Table 3. The structure of this MECP has

5

been optimized at the B3PW91-D3BJ level of theory, and the energy is shown in the Table. The MECP lies just half a kcal/mol above the quartet minimum, and including correction for zpe, it even lies very slightly lower in energy. In the case of CO, the spin needs to change from S = 2 to S = 0, which in principle could take place either in two steps *via* the triplet, or in a single step. We have previously[34] found that the two-step route is no lower in energy than the single step. Accordingly, we consider the direct route through ^{1,5}MECP CO in Table 3. This has been determined to lie 1.9 kcal/mol above the quintet minimum – similar to the energy gap of 2.4 kcal/mol relative to separate reactants reported previously.[34] However, due to the attractive dispersion interactions, it now lies *lower* than the separate ^{5}heme + CO. This might appear to change the reactivity pattern somewhat – however, for the rate constant for binding, what matters is the energy difference between the MECP and the geminal pair CO-heme with the CO in the pocket above the heme group. This remains positive in both sets of calculations, because of the already mentioned dispersively bound minimum.

Rate constants are calculated using NATST. Vibrational frequencies have been computed for the system within the seam of crossing between the relevant surfaces, using the methodology described previously. In our previous work,[33] the spin-orbit coupling matrix element between the electronic wavefunctions has been estimated, with the two-electron flip for ^{1,5}MECP CO taken to lead to a smaller matrix element (10 cm^{-1}) than the one-electron flip for 2,4-MECP NO (100 cm^{-1}). The reasons for this are (i) that in the CO case, the matrix element is a two-electron term which is less straightforward to calculate, and (ii) even the heme model system included in the present calculations is quite large. Here, we have used small configuration interaction (CI) wavefunctions expanded either in CASSCF or DFT orbitals together with an atomic mean-field spin-orbit coupling Hamiltonian to estimate the coupling. For the two-electron coupling at the ^{1,5}MECP, we have used the approximation[54] $^{1,5}H_{SOC} = {}^{1,3}H_{SOC} \times {}^{3,5}H_{SOC} / \Delta E$, where $^{3,5}H_{SOC}$ denotes the coupling element between the corresponding states, and ΔE is the energy gap between the degenerate singlet and quintet states, and the slightly higher triplet. Somewhat counter-intuitively, and contrary to previous assumptions, the singlet-quintet coupling for the ^{1,5}MECP with CO (55 cm^{-1}) emerges as not much smaller than the doublet-quartet coupling at the NO ^{2,4}MECP (172 cm^{-1}). The reason for this is that for the CO case, all three wavefunctions are essentially d^6 Fe(II) in character, and the 1,3- and 3,5-couplings broadly correspond to symmetry-allowed terms for spin-orbit coupling. For the NO MECP, on the other hand, the quartet and doublet wavefunctions both have mixed character, with some weight for configurations described as Fe(III)-NO^{-1}, which lead to large contributions to the SOC matrix element, but also significant weight for configurations with triplet Fe(II) character coupled to doublet NO either ferromagnetically or anti-ferromagnetically. The change in spin for these last terms is not accompanied by any change in the spatial orbitals, so contributes much less to the spin-orbit coupling. Different calculations yield different relative weights for these two types of wavefunction, and hence different SOC matrix elements. The

value reported above is most reliable based on involving the closest match to the DFT orbitals used in the MECP optimization, but other calculations yield somewhat lower values.

The quasi-harmonic method[55] with a cut-off of 50 cm^{-1} has been used to calculate vibrational contributions for the different species, including the MECP and the heme-XO encounter complexes in their ground states (quintet for CO, quartet for NO). In previous work,[33] the heme—XO encounter complex was treated as involving a heme group (with its harmonic frequencies), together with a free rotor CO molecule confined to a cubic box, with an approximate edge length of 3 Å. This second approach is in some ways more faithful to the picture emerging from the MD simulations, in which the XO ligand interacts loosely through van der Waals interactions with the heme group, but can translate and rotate. As the corresponding (quasi-)harmonic frequencies for the complexes are small, indicating considerable freedom for the XO ligand also in this approach. Nevertheless, inspection of the results suggests that the quasi-harmonic approach underestimates the partition function for the encounter complex, leading to binding rate constants k_2 that are too large. Accordingly, in the final approach used here, the partition function for the encounter complex is obtained by replacing three quasi-harmonic frequencies by translational partition functions with a box of 3 Å length. As for uncertainties in the calculated DFT energies and for the spin-orbit coupling matrix elements, this however introduces some uncertainty in the calculated rate constants. The slopes of the potential energy surfaces at the MECP and the reduced mass of the motion orthogonal to the crossing seam are obtained from the DFT calculations.

The above protocol returns room temperature rate constants k_2 of 7.1×10^7 s^{-1} and 7.6×10^9 s^{-1} for CO and NO binding, respectively. The value for CO is larger than that of 10^6 s^{-1} reported previously[33], with the difference due to the larger SOC matrix element, slight differences in the vibrational frequencies and relative energy for the MECP, and to the treatment of the partition function for the reactant state. The difference is however within the error bars for the calculations, especially considering the uncertainties in the calculated potential energy surfaces. Notable is that k_2 is much larger than k_{-1} in the case of NO, but slightly smaller in the case of CO. The uncertainty in the spin-orbit coupling matrix element in the case of NO was noted above; using a much smaller value of 50 cm^{-1} leads to a reduced rate constant of 1.2×10^9 s^{-1} , still significantly larger than k_{-2}. This implies that for NO, the rate-limiting step for binding is diffusion into the binding pocket, and the apparent rate constant should be the corresponding rate constant k_1. As discussed above, the MD simulations return $k_1 = 4.7 \times 10^8$ M^{-1} s^{-1}. Experimentally, a rate constant of 2.2×10^7 M^{-1} s^{-1} has been measured for NO binding to wild-type myoglobin[9], and our result is in fair agreement with this.

For CO, the second step is predicted to be rate-limiting, though only just. Assuming a larger difference between k_2 and k_{-1}, the apparent rate constant for reaction is then given by $k_1 \times k_2 / k_{-1}$,

which with the values calculated here is equal to 2.1×10^7 M^{-1} s^{-1}, again in fair agreement (given the uncertainties in the potential energy surfaces) with the measured rate constant which has been reported as 6.7×10^5 M^{-1} $s^{-1,[56]}$ or 5.1×10^5 M^{-1} $s^{-1,[9]}$.

Table 4. Calculated rate constants (k_2 and k_{-2}) for the spin-forbidden chemical reaction and calculated apparent rate constants for NO and CO binding to myoglobin.

ligand	k_2 (M^{-1} s^{-1})	k_{-2} (s^{-1})	k_{on} (M^{-1} s^{-1})	k_{off} (s^{-1})
CO	$7.1 \cdot 10^7$	0.9	$2.1 \cdot 10^7$	0.9
NO	$1.2 \cdot 10^9$	$2.0 \cdot 10^7$	$4.7 \cdot 10^8$	$3.0 \cdot 10^6$

The difference in rate-limiting step fits well with the observed very different volume profiles for the CO and O_2 binding reactions, as determined from high-pressure rate constant measurements.[56] To our knowledge, no activation volume has been measured in the case of NO, but the behavior of O_2 should be similar and is used here for reference. For O_2, the activation volume is small but positive ($+4.6$ cm^3 mol^{-1}), consistent with no change in spin state and a slight expansion to allow diffusion. For CO, on the other hand, a negative value of -9.2 cm^3 mol^{-1} is obtained, consistent with partial change of spin and hence contraction of the iron coordination sphere at the MECP.

Our calculations also lead to predicted rate constants for *release* of CO and NO. For CO, Fe-C bond breaking should be rate-determining, so the apparent rate constant for CO release should be k_{-2}, while for NO, subsequent diffusion should be rate determining, i.e. the apparent rate constant should be k_{-2} / k_2 × k_{-1}. From the energies in Table 3 and the NATST approach, k_{-2} values of 0.9 s^{-1} and 2.0×10^7 s^{-1} for CO and NO are respectively obtained. For CO, the rate constant for unbinding has been measured as 0.03 $s^{-1,[56]}$ or 0.02 $s^{-1,[9]}$, and our calculated value is in fair agreement with these values. For NO, we are not aware of a reported experimental rate constant for release for myoglobin, but values for guanylate cyclase and hemoglobin of the order of 10^{-5} s^{-1} have been reported. Our calculations imply a much larger apparent k_{off} value of 3.0×10^6 s^{-1}. This implies that the calculated relative energy for the bound NO form of -21.2 kcal/mol is too small, and that it should be instead in the region of -34 kcal/mol. Indeed, in earlier work,[49][53,57] CCSD(T) calculations implied that DFT significantly underestimates the bond energy for NO.

Conclusions

In the study the binding and loss of nitric oxide and carbon-monoxide to myoglobin was studied using molecular dynamics simulations, DFT calculations and non-adiabatic transition state theory. Combining the molecular dynamics simulations with the

NATST enabled us to treat both the diffusion of the ligand into the heme pocket and the spin-forbidden reaction step in which it binds to iron. This allows us to obtain an integrated overview of the whole ligand-binding process.

The MD simulations show that the rate of ligand diffusion is somewhat dependent on the solvent model used. While this is not a major concern in the present study, since larger errors occur elsewhere in our modeling, this is worthy of notice for other studies focusing only on the ligand entry steps. Also, our calculations show that CO entry into the heme pocket occurs slightly more slowly than NO entry, perhaps due to the slightly larger van der Waals radii of the atoms in CO compared to those of NO. The calculations also lead to predicted 'binding' constants $K_1 = k_1/k_{-1}$ for NO and CO within the heme pocket of the order of 1 M^{-1}. This implies that the hypothetical geminal pair species would be in equilibrium with separate XO in solution at about 1 M concentration. Given the much smaller volume of the heme pocket compared to the average molecular volume spanned by the XO molecules in 1 M solutions, this implies that XO is slightly stabilized in the heme pocket. We note again that CO is bound slightly more weakly than NO.

NATST calculations provide rate constants for the chemical spin-forbidden binding and release of the ligand within the heme pocket. Combined with the entry and exit rate constants, these provide an overall profile for the whole ligand binding event. The rate-limiting steps for NO and CO binding are predicted to be different: diffusion in the case of NO and spin-forbidden bond formation with Fe in the case of CO. This matches predictions based on experiments such as analysis of the volume profiles. The predicted overall rate constants agree with experiment to better than two orders of magnitude, which is reasonable given the approximations in the theory and the possible errors in the potential energy surfaces. In the case of CO, the NATST-predicted release rate constant also matches experiment fairly well, while for NO, it is predicted to be much too large, suggesting that the B3PW91-D3BJ functional does not describe the Fe−NO bond energy accurately, in agreement with previous work.

Overall, combining MD simulations with electronic structure theory calculation of potential energy surfaces for bond forming steps and statistical rate theory provides a satisfying overall picture of a complex process. This protocol could also be applied to other protein reactions, such as enzyme catalysis.

Computational Details

Molecular dynamics simulations (MD).

System setup. The crystal structure of the deoxy horse heart myoglobin was used (PDB code: 2FRK[58]) as a starting structure for the MD simulations. The protonation state of the titratable residues under neutral pH were predicted using the H++ webserver.[59–61] Based on the estimated pKa values His_{36} was doubly protonated. After visual inspection of the structure His_{24} and His_{93} were protonated on the δ nitrogen atom and all other histidines residues were protonated on the ε nitrogen atom. Hydrogen atoms were added using the standard

CHARMM protocol.[62] The protein was solvated by TIP3P water molecules arranged in a cubic box, with the edge of the box being at least 10 Å away from any point of the protein. One sodium ion was placed into the bulk solvent phase in order to neutralize the net charge of the system. The structure of the prepared system was energy-minimized in order to eliminate bad initial contacts. In the NPT ensemble using periodic boundary conditions (PBC) and the particle mesh Ewald (PME) summation method, the system was heated from 210 K to 310 K in 100 ps and finally it was equilibrated at the desired temperature for 1 ns. The CHARMM27 force field and the CHARMM39 software package were used for these simulations. The final structure had a secondary structure root-mean-square deviation (RMSD) of 0.753 Å with respect to the crystal structure.

Production run. The final structure obtained from the equilibration was used as the starting conformation for further simulations. The protein was re-solvated by TIP3P, TIP4P, TIP4Pew,[45] TIP4P/2005[44] and OPC[63] water molecules arranged in a dodecahedral box with edges at least 10 Å away from any point of the protein. 40 NO or CO molecules were placed in the bulk phase by refilling solvent holes resulting in an NO / CO concentration of approximately 0.29 M. (see Table S3 for more details) This concentration is high compared to the physiological concentration of NO or CO, but using this higher concentration a better sampling of diffusion events could be achieved. Furthermore, similarly high concentrations were used by Blumberger et al showing that up to about 0.500M the kinetics of ligand diffusion is independent of the concentration.[47][15] The total charge of the systems was neutralized using a single sodium ion. Energy minimization of these structures was followed by sequential relaxation of the constraints on protein atoms in three steps (each of 100 ps). Trajectories of 300 ns NPT simulations at 310 K and 1 bar were recorded for further analysis (collecting snapshots every 4ps). In the case of CO ligand with the OPC water model the simulation was run for 635 ns. For these simulations the GROMACS program was used[64] with the CHARMM27 force field for the protein atoms, sodium ion and water molecules, and recent three-site parameter models for the NO[65] and CO[24] molecules. The overall architecture of the protein did not change in the simulations, as it is also witnessed by the calculated backbone RMSD values that are reported in the SI in Table S2 (all values are below 1.6 Å).

Diffusion rate calculation in enzyme. As we wanted to study the diffusion of NO from the bulk phase to the active site of the protein and vice versa, therefore we assigned one of the following three states to each NO/CO molecule in every frame of the productive MD simulations. The heme pocket is bordered by Phe43, His64, Vla68, Leu29; Ile107 residues. Therefore, we took the center of mass the sidechains of these residues (r_{heme}) and if the center of mass ($r_{XO,i}^{mc}$), of any XO (CO or NO) molecule was within 3 Å from this center of mass, the ligand was assigned to be in the heme pocket. The XO molecule was assigned to be in the "protein" if it was not in the heme pocket, and it was within 6 Å from any of the protein heavy atoms ($r_{protein,j}$). In all other cases the ligand was assigned to be in the solvent phase. The definitions for the three states:

"heme pocket": $\quad d(r_{NO,i}^{mc}-r_{Fe}) < 3$ Å $\hfill$ (Eq. 1)

"protein": $\quad d(r_{NO,i}^{mc}-r_{Fe}) \geq 3$ Å $\quad$ and $\quad d(r_{NO,i}^{mc}-r_{protein,j}) < 6$ Å $\hfill$ (Eq. 2)

"solvent": $\quad d(r_{NO,i}^{mc}-r_{Fe}) \geq 3$ Å $\quad$ and $\quad d(r_{NO,i}^{mc}-r_{protein,j}) \geq 6$ Å $\hfill$ (Eq. 3)

This resulted in a 75,000 x 40 matrix for each productive MD simulations. Using these, the number of the events when an NO molecule entered from the solvent phase to the heme pocket ("in"-event: solvent→protein→heme pocket) could be determined, as well as the number of events when the NO molecule left ("out"-event: heme pocket→protein→solvent).

Kinetic model. Details of the kinetic model are provided in the Supporting information. We describe the ligand binding mechanism of NO/CO to myoglobin (Mb) system with a simple, two-step consecutive model as shown in Fig. 1.

In order to obtain the rate constant for the diffusion of NO into the pocket (k_1) and out of the pocket(k_{-1}), we use the number of "in-and-out" events, as at equilibrium the number of in and out events are equal::

$$\frac{d[XO]_{in}}{dt} = -k_1[Mb][XO] = \frac{N^o_{in-out}}{N_A} \cdot \frac{1}{t \cdot V} \qquad \text{(Eq. 4)}$$

$$\frac{d[XO]_{out}}{dt} = -k_{-1}[Mb\cdots XO] = \frac{N^o i_{in-out}}{N_A} \cdot \frac{1}{t_{XO,pocket} \cdot V} \qquad \text{(Eq. 5)}$$

where N^o_{in-out} refers to the number of events when an XO molecule reaches the active site from the solvent phase and returns there, N_A is Avogadro's number, t the simulation time (300 ns) and $t_{XO,pocket}$ the time that the ligands spends in the heme pocket, V the average volume of the unit cell ($\sim 2.4 * 10^{-22}$ dm^3, slightly dependent upon the water model) during the simulation, respectively. After substituting the corresponding values in to Eq. 4 and 5. one can obtain the values of k_1 and k_{-1}.

Quantum-chemical calculations. The histidine-ligated heme enzyme was modelled as a bare porphyrin-imidazole complex to which the NO and CO ligands were added. The ligand-free porphyrin-imidazole complex and the CO adduct were modelled in the singlet, triplet and quintet spin states, while the NO adduct was described using the doublet, quartet and sextet spin states. Based on previous gas phase calculations,[49] the B3PW91 functional was used and test calculations were used to determine a flexible yet compact basis set that reproduces results obtained with very large polarized and augmented triple-zeta basis sets. Therefore, both geometries and vibrational frequencies were determined using the 6-311+G(d) basis set for Fe and the XO ligand and the 6-31G(d) basis for the other atoms. Care was taken to locate the structure and electronic structure of lowest energy for each spin state, taking into account also C_S symmetry where appropriate. Geometries were optimized using the Gaussian09 program package[66] with Grimme's D3 empirical dispersion correction including Becke-Johnson damping.[67] In-house developed codes were used for the localization of MECPs[68], for the vibrational frequency analysis at these points (GlowFreq)[69,70] and for the NATST calculations.[71] Spin-orbit coupling matrix elements were calculated in the Molpro 2015 program package[72,73] using the atomic mean-field approximation.[74] Details of these calculations are in the supporting information.

Acknowledgements

Supporting information

Details of the spin-orbit coupling calculations, of the kinetic model used in the study, occupation of pockets by ligands within myoglobin, ligand and enzyme concentrations, RMS deviation of protein backbone during the simulations and Cartesian coordinates of the located stationary points and MECPs are provided as supporting information.

**Keywords:** spin-forbidden, heme, ligand binding, molecular dynamics, quantum chemistry

References

[1] K. P. Kepp, *Coord. Chem. Rev.* **2017**, *344*, 363–374.

[2] K. P. Kepp, *ChemPhysChem* **2013**, *14*, 3551–3558.

[3] T. Shimizu, D. Huang, F. Yan, M. Stranava, M. Bartosova, V. Fojtíková, M. Martínková, *Chem. Rev.* **2015**, *115*, 6491–6533.

[4] J. C. Toledo, O. Augusto, *Chem. Res. Toxicol.* **2012**, *25*, 975–989.

[5] M. Kajimura, R. Fukuda, R. M. Bateman, T. Yamamoto, M. Suematsu, *Antioxid. Redox Signal.* **2010**, *13*, 157–92.

[6] M. Silatani, F. A. Lima, T. J. Penfold, J. Rittmann, M. E. Reinhard, H. M. Rittmann-Frank, C. Borca, D. Grolimund, C. J. Milne, M. Chergui, *Proc. Natl. Acad. Sci. U. S. A.* **2015**, *112*, 12922–7.

[7] C. R. Andrew, O. N. Petrova, I. Lamarre, J.-C. Lambry, F. Rappaport, M. Negrerie, *ACS Chem. Biol.* **2016**, *11*, 3191–3201.

[8] E. G. Moore, Q. H. Gibson, *J. Biol. Chem.* **1976**, *251*, 2788–2794.

[9] F. Draghi, A. E. Miele, C. Travaglini-Allocatelli, B. Vallone, M. Brunori, Q. H. Gibson, J. S. Olson, *J. Biol. Chem.* **2002**, *277*, 7509–7519.

[10] E. Martin, V. Berka, E. Bogatenkova, F. Murad, A.-L. L. Tsai, *J. Biol. Chem.* **2006**, *281*, 27836–27845.

[11] Y. Zhao, P. E. Brandish, D. P. Ballou, M. A. Marletta, *Proc. Natl. Acad. Sci. U. S. A.* **1999**, *96*, 14753–14758.

[12] V. G. Kharitonov, V. S. Sharma, D. Magde, D. Koeslin, *Biochemistry* **1997**, *36*, 6814–6818.

[13] V. G. Kharitonov, M. Russwurm, D. Magde, V. S. Sharma, D. Koesling, *Biochem. Biophys. Res. Commun.* **1997**, *239*, 284–286.

[14] T. E. Carver, R. J. Rohlfs, J. S. Olson, Q. H. Gibson, R. S. Blackmore, B. A. Springer, S. G. Sligar, *J. Biol. Chem.* **1990**, *265*, 20007–20020.

[15] D. De Sancho, A. Kubas, P.-H. H. Wang, J. Blumberger, R. B. Best, *J. Chem. Theory Comput.* **2015**, *11*, 1919–1927.

[16] M. M. Teeter, *Protein Sci.* **2004**, *13*, 313–318.

[17] J. Z. Ruscio, D. Kumar, M. Shukla, M. G. Prisant, T. M. Murali, A. V. Onufriev, *Proc. Natl. Acad. Sci.* **2008**, *105*, 9204–9209.

[18] K. Nienhaus, P. Deng, J. M. Kriegl, G. U. Nienhaus, *Biochemistry* **2003**, *42*, 9647–9658.

[19] Karin Nienhaus, Andreas Ostermann, G. Ulrich Nienhaus, Fritz G. Parak, Marius Schmidt, *Biochemistry* **2005**, *44*, 5095–5105.

[20] K. N. Woods, *Soft Matter* **2014**, *10*, 4387–4402.

[21] Y. Nishihara, S. Kato, S. Hayashi, *Biophys. J.* **2010**, *98*, 1649–1657.

[22] Adam Kubas, C. Orain, D. De Sancho, L. Saujet, M. Sensi, C. Gauquelin, P. S. Isabelle Meynial-Salles, H. Bottin, C. Baffert, V. Fourmond, et al., *Nat. Chem.* **2017**, *9*, 88–95.

[23] P. Wang, R. B. Best, J. Blumberger, *J. Am. Chem. Soc.* **2011**, *133*, 3548–3556.

[24] P. Wang, J. Blumberger, *Proc. Natl. Acad. Sci. U. S. A.* **2012**, *109*, 6399–6404.

[25] M. Radoń, *J. Chem. Theory Comput.* **2014**, *10*, 2306–2321.

[26] A. R. Groenhof, M. Swart, A. W. Ehlers, K. Lammertsma, *J. Phys. Chem. A* **2005**, *109*, 3411–3417.

[27] V. K. K. Praneeth, F. Neese, N. Lehnert, *Inorg. Chem.* **2005**, *44*, 2570–2572.

[28] B. B. Wayland, L. W. Olson, *J. Am. Chem. Soc.* **1974**, *96*, 6037–6041.

[29] M. Radón, E. Broclawik, K. Pierloot, *J. Phys. Chem. B* **2010**, *114*, 1518–1528.

[30] K. P. Jensen, U. Ryde, *J. Biol. Chem.* **2004**, *279*, 14561–14569.

[31] M. Radoń, K. Pierloot, *J. Phys. Chem. A* **2008**, *112*, 11824–11832.

[32] N. Strickland, J. N. Harvey, *J. Phys. Chem. B* **2007**, *111*, 841–52.

[33] J. N. Harvey, *Faraday Discuss.* **2004**, *127*, 165–177.

[34] J. N. Harvey, *J. Am. Chem. Soc.* **2000**, *122*, 12401–12402.

[35] M. Brunori, Q. H. Gibson, *Embo R.* **2001**, *21*, 674–679.

[36] E. E. Scott, Q. H. Gibson, J. S. Olson, *J. Biol. Chem.* **2001**, *276*, 5177–88.

[37] J. S. Olson, J. Soman, G. N. Phillips, *IUBMB Life* **2007**, *59*, 552–562.

[38] F. Schotte, M. Lim, T. A. Jackson, A. V Smirnov, J. Soman, J. S. Olson, G. N. Phillips, M. Wulff, P. A. Anfinrud, *Science (80-.).* **2003**, *300*, 1944–1947.

[39] D. R. Nutt, M. Meuwly, *Proc. Natl. Acad. Sci. U. S. A.* **2004**, *101*, 5998–6002.

[40] J. Cohen, A. Arkhipov, R. Braun, K. Schulten, *Biophys. J.* **2006**, *91*, 1844–1857.

[41] R. F. Tilton, I. D. Kuntz, G. A. Petsko, *Biochemistry* **1984**, *23*, 2849–2857.

[42] C. Bossa, A. Amadei, I. Daidone, M. Anselmi, B. Vallone, M. Brunori, A. Di Nola, A. Di Nola, *Biophys. J.* **2005**, *89*, 465–474.

[43] X. Huang, S. G. Boxer, *Nat. Struct. Mol. Biol.* **1994**, *1*, 226–229.

[44] J. L. F. Abascal, C. Vega, *J. Chem. Phys.* **2005**, *123*, 234505.

[45] H. W. Horn, W. C. Swope, J. W. Pitera, J. D. Madura, T. J. Dick, G. L. Hura, T. Head-Gordon, *J. Chem. Phys.* **2004**, *120*, 9665–9678.

[46] S. Izadi, R. Anandakrishnan, A. V Onufriev, **n.d.**, DOI 10.1021/jz501780a.

[47] P.-H. Wang, D. De Sancho, R. B. Best, J. Blumberger, in *Methods Enzymol.*, Academic Press, **2016**, pp. 299–326.

[48] J. N. Harvey, *Phys. Chem. Chem. Phys.* **2007**, *9*, 331–43.

[49] J. Oláh, J. N. J. N. Harvey, *J. Phys. Chem. A* **2009**, *113*, 7338–45.

[50] J. C. Lorquet, B. Leyh-Nihantt, *J. Phys. Chem* **1988**, *92*, 4778–4783.

[51] S. Franzen, *Proc. Natl. Acad. Sci. U. S. A.* **2002**, *99*, 16754–9.

[52] S. Franzen, *J. Phys. Chem. B* **2002**, *106*, 4533–4542.

[53] P. E. M. Siegbahn, M. R. A. Blomberg, S. Chen, *J. Chem. Theory Comput.* **2010**, *6*, 2040–2044.

[54] E. Buhks, G. Navon, M. Bixon, J. Jortner, *J. Am. Chem. Soc.* **1980**, *102*, 2918–2923.

[55] R. F. Ribeiro, A. V. Marenich, C. J. Cramer, D. G. Truhlar, *J. Phys. Chem. B* **2011**, *115*, 14556–14562.

[56] S. Adachi, I. Morishima, *J. Biol. Chem.* **1989**, *264*, 18896–18901.

[57] M. Radoń, K. Pierloot, *J. Phys. Chem. A* **2008**, *112*, 11824–32.

[58] D. M. Copeland, A. S. Soares, A. H. West, G. B. Richter-Addo, *J. Inorg. Biochem.* **2006**, *100*, 1413–1425.

[59] R. Anandakrishnan, B. Aguilar, A. V Onufriev, *Nucleic Acids Res.* **2012**, *40*, W537-541.

[60] J. Myers, G. Grothaus, S. Narayanan, A. Onufriev, *Proteins* **2006**, *63*, 928–938.

[61] J. C. Gordon, J. B. Myers, T. Folta, V. Shoja, L. S. Heath, A. Onufriev, *Nucleic Acids Res.* **2005**, *33*, W368-371.

[62] B. R. Brooks, C. L. Brooks, A. D. Mackerell, L. Nilsson, R. J. Petrella, B. Roux, Y. Won, G. Archontis, C. Bartels, S. Boresch, et al., *J. Comput. Chem.* **2009**, *30*, 1545–1614.

[63] S. Izadi, R. Anandakrishnan, A. V. Onufriev, *J. Phys. Chem. Lett.* **2014**, *5*, 3863–3871.

[64] S. Pronk, S. Pall, R. Schulz, P. Larsson, P. Bjelkmar, R. Apostolov, M. R. Shirts, J. C. Smith, P. M. Kasson, D. van der Spoel, et al., *Bioinformatics* **2013**, *29*, 845–854.

[65] M. Meuwly, O. M. Becker, R. Stote, M. Karplus, *Biophys. Chem.* **2002**, *98*, 183–207.

[66] M. J. Frisch, G. W. Trucks, H. B. Schlegel, G. E. Scuseria, M. A. Robb, J. R. Cheeseman, G. Scalmani, V. Barone, B. Mennucci, G. A. Petersson, et al., *Gaussian 09, Revis. E.01, Gaussian, Inc., Wallingford CT* **2009**.

[67] S. Grimme, S. Ehrlich, L. Goerigk, *J. Comput. Chem.* **2011**, *32*, 1456–1465.

[68] J. N. Harvey, M. Aschi, H. Schwarz, W. Koch, *Theor. Chem. Accounts Theory, Comput. Model. (Theoretica Chim. Acta)* **1998**, *99*, 95–99.

[69] K. L. Gannon, M. A. Blitz, C.-H. Liang, M. J. Pilling, P. W. Seakins, D. R. Glowacki, J. N. Harvey, *Faraday Discuss.* **2010**, *147*, 173–188.

[70] J. M. C. Plane, C. L. Whalley, L. Frances-Soriano, A. Goddard, J. N. Harvey, D. R. Glowacki, A. A. Viggiano, *J. Chem. Phys.* **2012**, *137*, 14310.

[71] J. N. Harvey, M. Aschi, *Faraday Discuss.* **2003**, *124*, 129.

[72] H.-J. Werner, P. J. Knowles, G. Knizia, F. R. Manby, M. Schütz, *Wiley Interdiscip. Rev. Comput. Mol. Sci.* **2012**, *2*, 242–253.

[73] MOLPRO, version 2015.1, a package of ab initio programs, H.-J. Werner, P. J. Knowles, G. Knizia, F. R. Manby, M. Schütz, P. Celani, W. Györffy, D. Kats, T. Korona, R. Lindh, A. Mitrushenkov, G. Rauhut, K. R. Shamasundar, T. B. Adler, R. D. Amos, A. Bernhardsson, A. Berning, D. L. Cooper, M. J. O. Deegan, A. J. Dobbyn, F. Eckert, E. Goll, C. Hampel, A. Hesselmann, G. Hetzer, T. Hrenar, G. Jansen, C. Köppl, Y. Liu, A. W. Lloyd, R. A. Mata, A. J. May, S. J. McNicholas, W. Meyer, M. E. Mura, A. Nicklass, D. P. O'Neill, P. Palmieri, D. Peng, K. Pflüger, R. Pitzer, M. Reiher, T. Shiozaki, H. Stoll, A. J. Stone, T. Tarroni, T. Thorsteinsson, and M. Wang, see http://www.molpro.net.}

[74] B. A. Heß, C. M. Marian, U. Wahlgren, O. Gropen, *Chem. Phys. Lett.* **1996**, *251*, 365–371.

Entry for the Table of Contents

FULL PAPER
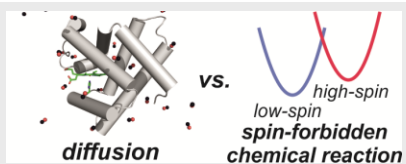
Anikó Lábas, Dóra K. Menyhárd, Jeremy N. Harvey,* Julianna Oláh*

Page No. – Page No.
First principles calculation of the reaction rates for ligand binding to myoglobin: the cases of NO and CO

Molecular dynamics simulations, DFT calculations in conjunction with statistical rate theory are used to predict the rate constants for CO and NO binding by myoglobin. This combination of methods provides an integrated view of the whole ligand-binding process and the overall rate constants agree with experiment to better than two orders of magnitude.